A&A 423, 121–132 (2004)
DOI: 10.1051/0004-6361:20035912

Astronomy & Astrophysics

VLT/ISAAC spectra of the Hβ region in intermediate redshift quasars*,**

J. W. Sulentic[1], G. M. Stirpe[2], P. Marziani[3], R. Zamanov[3,4], M. Calvani[3], and V. Braito[3,5]

[1] Department of Physics and Astronomy, University of Alabama, Tuscaloosa, AL 35487, USA
e-mail: giacomo@merlot.astr.ua.edu
[2] Osservatorio Astronomico di Bologna, INAF, via Ranzani 1, 40127 Bologna, Italy
e-mail: giovanna.stirpe@bo.astro.it
[3] Osservatorio Astronomico di Padova, INAF, Vicolo dell' Osservatorio 5, 35122 Padova, Italy
e-mail: [marziani; zamanov; calvani]@pd.astro.it
[4] Astrophysics Research Institute, Liverpool John Moores University, Twelve Quays House, Egerton Wharf, Birkenhead CH41 1LD, UK
e-mail: rz@astro.livjm.ac.uk
[5] Osservatorio Astronomico di Brera, INAF, via Brera 28, 20121 Milano, Italy
e-mail: braito@brera.mi.astro.it

Received 19 December 2003 / Accepted 4 May 2004

Abstract. We present high *S/N* spectra of the Hβ region in 17 intermediate redshift ($0.85 \leq z \leq 2.5$) quasars. The spectra represent first results of our campaign to test the redshift/luminosity robustness of the so-called Eigenvector 1 (E1) parameter space as developed for low redshift AGN in Sulentic et al. (2000, ApJ, 536, L5). The new quasars span the luminosity range $-26 \geq M_B \geq -29$ while most of our low redshift sample ($n = 215$) involve sources in the range $-19 \geq M_B \geq -26$. The high redshift sources show E1 parameter values and domain occupation that are similar to our low redshift sample supporting earlier findings that E1 parameters are uncorrelated with source luminosity. Elementary accretion theory can account for a systematic increase of the minimum observed Hβ profile width with source luminosity. Narrow line Seyfert 1 sources with $M_B = -28$ show *FWHM*(Hβ) as much as 2000 km s^{-1} broader than those with $M_B = -22$. A possible change in the higher redshift/luminosity sources involves systematically weaker [OIII]$\lambda\lambda$4959,5007 narrow line emission.

Key words. line: profiles – galaxies: quasars: emission lines

1. Introduction

There is as yet no convincing evidence for strong spectral evolution in quasars especially as far as low-ionization emission lines (LIL) are concerned. Recent UV FeII observations suggests, for example, that FeII emission remains strong up to $z \approx 6.4$ (Barth et al. 2003; Freudling et al. 2003). The lack of spectral evolution may not present difficulties for quasar modeling per se but it may have serious cosmological implications (e.g., Hamann & Ferland 1999; Matteucci & Recchi 2001). In the modelling context see Zamanov & Marziani (2002) for a demonstration of self-similar properties in widely different accreting systems.

We have been searching for a parameter space to serve the role of the stellar H-R Diagram in discriminating quasar spectral phenomenology and evolutionary states. Our so-called Eigenvector 1 (E1) parameter space (Sulentic et al. 2000b, hereafter S00b) shows promise in this context (see e.g., Marziani et al. 2001; Sulentic et al. 2002; Marziani et al. 2003a). The optical E1 parameters involve broad line measures of the full width at half-maximum (*FWHM*) of the broad component of Hβ (H$\beta_{\rm BC}$) and the equivalent width ratio H$\beta_{\rm BC}$/FeII, where FeII is measured from the λ4570 blend. These are supplemented by measures of higher ionization CIVλ1549 line shift and the soft X-ray photon index making E1 a 4D parameter space. The distribution of sources in the E1 optical plane is consistent with a principal band or "main sequence" of source occupation. The shape of that principal sequence motivated an alternative suggestion that two AGN populations exist with an arbitrary separation at *FWHM* H$\beta_{\rm BC}$ = 4000 km s^{-1}. Population A sources generally show radio-quietness, strong optical FeII emission, a soft X-ray excess and a systematic CIV blueshift. Narrow line Seyfert 1 sources (NLSy1) represent an extreme of Population A which contains ~65% of all radio-quiet (RQ) sources (Marziani et al. 2003a). Population B sources generally show weaker FeII emission and no soft X-ray

* Based on observations collected at the European Southern Observatory, Chile. Proposal ref.: ESO 68.B–0364(A).
** Table 1 and Figs. 1 and 2 are only available in electronic form at http://www.edpsciences.org

excess or CIV blueshift. The latter population contains most radio-loud (RL) sources, and about 25% of the RQ sources. RL sources found in Population A are located there because of a preferred orientation to our line of sight (e.g. core-dominated radio emission; Sulentic et al. 2003). These properties have emerged from a growing sample ($N \geq 215$; Marziani et al. 2003b, hereafter M03b) of low redshift (mostly $z < 0.8$) AGN. Results so-far give us cautious optimism that source orientation can be decoupled from physics using E1 space (Marziani et al. 2001; Sulentic et al. 2003).

Our definition of E1 began with the low redshift part of the PG quasar sample (Boroson & Green 1992) and our optical E1 parameters emerged in their principal component analysis of the correlation matrix for the PG sample. Interestingly enough, source luminosity emerged in their second eigenvector implying that the E1 correlations are source luminosity independent at least at low z. We continue to find no evidence for correlations involving optical luminosity in E1 space. Radio luminosity is correlated but *only* in the sense that radio-loud AGN show significantly restricted domain space occupation (e.g. Population B). At the same time, sources with radio/optical flux ratio <10 (RQ) show no preferred domain space occupation in E1.

Naturally we would like to test the robustness of the E1 space using samples of sources with higher mean redshift and luminosity. This involves tests using samples of quasars with $z > 1.0$ and optical spectroscopy CIV and/or IR measures of the Hβ region. Recent Sloan Digital Sky Survey (SDSS) results for a large intermediate/high redshift sample (Richards et al. 2002) show CIV trends very similar to our low redshift (S00b) E1 results (i.e. 65−75% of sources with Population A CIV properties). IR spectra of the Hβ region, up to this point in time (e.g., Espey et al. 1989; Murayama et al. 1998; Oya et al. 1998; McIntosh et al. 1999, hereafter Mc99; but see Dietrich et al. 2002) have suffered from low resolution and *S/N* making comparisons with our E1 sample impossible. We have begun a campaign to obtain high *S/N* IR spectra of the region of the Hβ+optical FeIIλ4570 blend in intermediate redshift quasars. We present results from the reduction and analysis of ESO VLT1/ISAAC spectra for our first year sample of 17 sources. We show that the quality of these data is comparable to our low-redshift database (M03b). We are able to measure the H$\beta_{\rm BC}$ and Fe II$_{\rm opt}$ E1 parameters using the same techniques described in M03b (Sect. 2). We present an analysis of the luminosity and redshift trends using the new intermediate redshift IR and older low redshift optical data (Sect. 4.2). We also interpret the new line measures in the context of the E1 parameter space (Sect. 5.1).

2. Observations, data reduction, and measurements

Table 1 presents a summary of the observations and basic source properties, with footnotes giving detailed descriptions of each column. Data were collected using VLT1/ISAAC operated in service mode between 2001 November and 2002 February. All spectra were obtained with a slit width of 0.6 arcsec. Each spectrum corresponds to the wavelength range of an IR window (sZ, Z, J, H) and covers the region of redshifted Hβ and Fe IIλ4570 (or Fe IIλ5130 blend). Two matching spectra in adjacent bands were obtained in five cases, to improve the coverage of the Hβ spectral region.

Reductions were performed using standard IRAF routines. Sequences of frames with a given Detector Integration Time (DIT, see Table 1) were obtained with the source at different positions (e.g. A, B, C...) along the slit. All frames at a specific slit position were averaged and the average of observations at all other positions was subtracted from it. The resulting differences were divided by the appropriate flat field frames provided by the ESO pipeline reduction. Any residual background was then eliminated by fitting and subtracting a low-order polynomial function to each spatial line of the frame. Spectra were extracted using the IRAF program *apall.* Cosmic ray hits were eliminated by interpolation, comparing the affected spectrum with the other spectra of the same source. For each position along the slit a corresponding xenon/argon arc spectrum was extracted from the calibration frame, using the same extraction parameters. The wavelength calibration was well modeled by 3rd order Chebyshev polynomial fits to the positions of 15−30 lines, with rms residuals of 0.3 Å in the *Z* band, 0.4 Å in *sZ*, 0.6 Å in *J*, and 0.9 Å in *sH*. Once matched with the corresponding arc calibrations, the individual spectra of each source were rebinned to a common wavelength scale. They were then averaged with weights proportional to the total integration time of each spectrum.

The spectra of the atmospheric standard stars were extracted and wavelength-calibrated in the same way. All clearly identifiable stellar features (H and HeI absorption lines) were eliminated from the stellar spectra by spline interpolation of the surrounding continuum intervals. Each target spectrum was then divided by its corresponding standard star spectrum in order to correct for the atmospheric absorption features. This was achieved with the IRAF routine *telluric,* which allows one to optimize the correction with slight adjustments in shift and scaling of the standard spectrum. The shape of the continuum of the standard star was eliminated from the spectrum of each target by multiplying the latter with an artificial black-body continuum corresponding to the temperature of the star, determined on the basis of its tabulated spectral type. Finally, the correct flux calibration of each spectrum was achieved by scaling it according to the magnitude of the standard star and to the ratio of the respective DITs. Because the seeing almost always exceeded the width of the slit, significant light loss occurred, and therefore the absolute flux scale of the spectra is not to be considered as accurate. However, in this high-wavelength range we consider the light losses to be independent of wavelength, and they should therefore not affect the relative calibration of the spectra.

Redshift measures are usually based on [O III]λ5007 but the narrow component of Hβ (H$\beta_{\rm NC}$) was also used whenever possible. Redshift uncertainty is usually $\lesssim$150 km s^{-1}, including estimated uncertainty of the wavelength calibration. These measures can be regarded as the most accurate available, with the caveat that some (Population A) sources with narrowest *FWHM* H$\beta_{\rm BC}$ sometimes show a significant [O III]$\lambda\lambda$4959,5007 blueshift (Zamanov et al. 2002; Marziani et al. 2003a).

The *S/N* ratio has been estimated by: (1) locating a spectral region that is flat and free of strong lines and (2) dividing two times the rms scatter by the average signal in that region. Examination of the spectra will reveal the limited regions available for *S/N* and continuum estimation. *S/N* values are comparable to our low-redshift M03b data. The IR spectra presented in Figs. 1 and 2 are, on average, indistinguishable from the data in the M03b atlas. Spectral resolution is $FWHM = 9$ Å in the Z band ($\lambda_C \approx 9000$ Å), 11 Å in the sZ band ($\lambda_C \approx 10\,600$ Å), 12 Å in the J band ($\lambda_C \approx 12\,400$ Å), and 16 Å in the H band ($\lambda_C \approx 16\,000$ Å). In all bands this is equivalent to $FWHM \approx 300$ km s^{-1} which is similar to the resolution of the M03b data.

Measurements were carried out with exactly the same technique employed by M03b. The de-redshifted spectra were continuum- and then Fe II$_{opt}$-subtracted. The spectral width of the IR windows made continuum modeling and subtraction uncertain in many cases. The lowest regions in the adopted FeII fits shown in the spectra of Fig. 2 allow one to infer the adopted continuum level. Fe II$_{opt}$ subtraction was achieved employing a template based upon spectra of I Zw 1, scaled and broadened by fixed factors in a plausible range chosen by eye. The best Fe IIλ4570 template was chosen as the one yielding the minimum residual in a matrix of 10×10 scaling and broadening factors. An interesting result comes from the broadening factor of the Fe II$_{opt}$ template: an estimate of the intrinsic width of the individual Fe II$_{opt}$ lines. All measures have an accuracy (for a given *S/N*) similar to those in M03b. The Hβ_{BC} was isolated after subtracting the narrow component of Hβ_{NC} (self-consistent guidelines are provided in M03b). Both [O III]$\lambda\lambda$4959,5007 and He IIλ4686 were also measured whenever possible.

3. Sample considerations

We adopted the Hamburg-ESO (HE) quasar surveys (Wisotzki et al. 2000) for tests of E1 validity and robustness. The $U - B$ color-selected PG sample (Boroson & Green 1992) is thought to be biased towards selecting what we call extreme Population A sources i.e. NLSy1s ($FWHM$(Hβ_{BC}) $\lesssim$ 2000 km s^{-1}). We are in the process of observing both low and intermediate redshift subsamples of grism-selected HE quasars in order to evaluate effects of selection bias on mean E1 parameter values and E1 domain space occupation. The low redshift sample will compare E1 properties of HE grism- vs. PG color-selected quasars. The intermediate redshift sample will explore possible E1 changes with redshift/luminosity. If anything, the HE samples should be biased towards broader/stronger lined (Population B) quasars. The PG sample finds $20/87 \approx 23\%$ NLSy1s while the (also color-selected) SDSS (Williams et al. 2002) suggests that ∼15% of all low-redshift AGN are NLSy1. Our low redshift M03b sample includes 150 RQ and 65 RL sources. NLSy1, which are very rarely RL, account for 11% and 16%, respectively, of the total and RQ parts of our sample.

RL sources are over-represented (30%) in our sample because that part of our low-redshift sample has been surveyed more completely to our adopted magnitude limit $V = 16.5$. We find 85% RQ and 10% RL in the Population A domain while 37% RQ and 75% RL are found in the Population B domain. Only 7% of the sample fall off of the Population A-B "main sequence" and are designated "outliers". RL sources are defined as those with $R_K = f_{6\ cm}/f_B \gtrsim 100$, plus any sources near and below that limit showing double-lobed (FRII) radio morphology ($R_K \approx 70$–80; Sulentic et al. 2003). All true core-dominated RL sources are assumed to be radio flux-boosted FRII's and should show values of $R_K > 80$. The condition $R_K \gtrsim 80$ yields 4 RL sources in our VLT/ISAAC sample with two additional radio-intermediate sources with $10 \lesssim R_K \lesssim 80$. This implies an excess of RL sources in the intermediate-redshift sample; however it is premature to draw such conclusions. The small size of our new sample suggests that sources are best compared in terms of the so-called E1 Populations A and B. They are represented by 6 and 11 sources respectively.

Our comparisons with the low-z-defined E1, and search for luminosity effects, make use of the M03b dataset that includes 215 sources with a "core" of ≈85 sources from the PG survey (Boroson & Green 1992). In Marziani et al. (2003a) we increased our low-redshift sample by adding the soft-X-ray selected sources from Grupe et al. (1999). All defining properties of E1 space have remained stable as our sample has grown from 70 to >250 low-redshift sources. Strong luminosity effects were ruled out but luminosity dependence was not studied in detail. No claim of completeness can be made for the majority RQ part of the M03b sample (∼30%), however V/V_{max} tests suggest that the RL part is about 80% complete to $z \approx 0.8$; $m_V \approx 16.5$. However incompleteness is not a major impediment to a proper correlation analysis with M_B if we have uniform sampling across the entire absolute magnitude range. Figure 3 shows the M_B (Véron-Cetty & Véron 2000) and redshift distributions for the M03b and VLT samples. We also include the much lower *S/N* high-z observations from Mc99. The range $-20 \gtrsim M_B \gtrsim -29$ is reasonably well sampled. It is important to stress that, if RQ and RL sources are considered separately, most RQ fall in the range $-20 \gtrsim M_B \gtrsim -28$, while RL are on average more luminous, $-24 \gtrsim M_B \gtrsim -29$. We are observing the brightest sources in the HE survey which means that we are sampling an M_B range similar to Mc99 but with sources distributed over a wider range of redshift.

4. Results

Wavelength- and flux-calibrated spectra of the 17 HE quasars are shown in Figs. 1 and 2. Figures show de-redshifted spectra both before and after continuum and Fe II$_{opt}$ subtraction. The right-hand panels of Fig. 2 show the "cleaned" Hβ_{BC} profile following Hβ_{NC}, [O III]$\lambda\lambda$4959,5007 and He IIλ4686 subtraction. Rest-frame equivalent widths are given in Table 2 for Hβ_{BC}, Fe IIλ4570, Hβ_{NC} and [O III]$\lambda\lambda$4959,5007, along with the *FWHM* estimates for individual terms of the Fe IIλ4570 emission. *FWHM* and other Hβ_{BC} profile measures are provided in Table 3 along with 2σ uncertainties. Line parameters such as asymmetry index, kurtosis and line centroid at various fractional intensities are the same as defined in

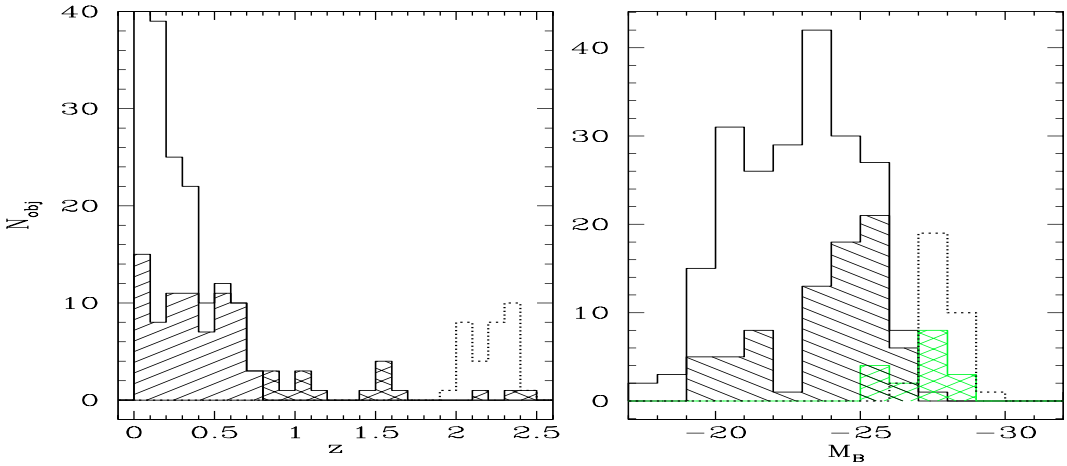

Fig. 3. Redshift (*left*) and absolute *B* magnitude (*right*) distributions for the total M03 sample (unhatched), for the RL subsample of M03 (hatched), for the 17 sources of this study (cross-hatched) and for the sources with $2.0 \lesssim z \lesssim 2.5$ studied by Mc99 (dotted line).

Table 2. Measurements of equivalent widths and *FWHM* of strongest lines.

Object name (1)	$W(\mathrm{H}\beta_{\mathrm{BC}})^a$ (2)	$W(\mathrm{Fe\,II}\lambda4570)^b$ (3)	$FWHM(\mathrm{Fe\,II}\lambda4570)^c$ (4)	$W(\mathrm{H}\beta_{\mathrm{NC}})^d$ (5)	$W([\mathrm{O\,III}]\lambda4959)^d$ (6)	$W([\mathrm{O\,III}]\lambda5007)^d$ (7)
HE0003−5026	81 ± 9	25 ± 10	5300 ± 3100	0.5 ± 0.3	0.98 ± 0.4	6.2 ± 0.7
HE0005−2355	74 ± 7	11 ± 7	7300 ± 4800	4.0 ± 0.6	11.9 ± 1.2	42.6 ± 4
HE0048−2804	102 ± 10	40 ± 15	10000 ± 2300	1.8 ± 0.9	6.5 ± 1	21.6 ± 2.2
HE0122−3759	41 ± 4	37 ± 5	2100 ± 1600	0	0 ± 1	3.0 ± 1
HE0205−3756	82 ± 10	34 ± 5	3600 ± 1800	0.8 ± 0.8	0.4 ± 0.3	2.0 ± 1.5
HE0248−3628	47 ± 5	20 ± 3	4500 ± 2300	1.1 ± 0.4	...[e]	3.7 ± 1
HE0331−4112	72 ± 8	38 ± 7	3800 ± 2300	0.5 ± 0.5	2.1 ± 0.5	4.7 ± 0.5
HE0349−5249	82 ± 9	28 ± 3	2800 ± 1600	0.4 ± 0.4	0 ± 1	1.3 ± 0.6
HE0353−3919	70 ± 20	40 ± 20	4800 ± 2600	0	0	0
HE0454−4620	53 ± 6	10 ± 10	...	0	13.7 ± 2	36.4 ± 4
HE2202−2557	45 ± 5	20 ± 3	5500 ± 2600	1.25 ± 0.4	3 ± 1	8.7 ± 0.9
HE2259−5524	92 ± 10	68 ± 15	2700 ± 1600	0	0	0
HE2305−5315	48 ± 5	40 ± 15	1800 ± 1300	0	0	0
HE2340−4443	78 ± 8	13 ± 3	4800 ± 2600	2.4 ± 0.8	6.6 ± 0.7	15 ± 1.5
HE2349−3800	60 ± 6	24 ± 4	3800 ± 2100	2.1 ± 0.7	1.0 ± 0.2	8.9 ± 0.9
HE2352−4010	51 ± 5	21 ± 3	1300 ± 1300	0	0	2.0 ± 1.0
HE2355−4621	88 ± 9	12 ± 2	6300 ± 2800	2.4 ± 0.8	3.75 ± 0.5	17.1 ± 2

[a] Rest frame equivalent width of Hβ_{BC} in Å $\pm 2\sigma$ confidence level uncertainty.
[b] Rest frame equivalent width of the Fe IIλ4570 blend in Å $\pm 2\sigma$ confidence level uncertainty.
[c] *FWHM* of lines in the Fe IIλ4570 blend and uncertainty at 2σ, in km s^{-1}. See text for details.
[d] Rest frame equivalent width of Hβ_{NC}, [O III]λ4959, and [O III]λ5007 in Å, with uncertainty at 2σ.
[e] [O III]λ4959 not visible. [O III]λ5007 is instead well visible.

Marziani et al. (1996) (hereafter M96) and M03b. Asymmetry index is defined as:

$$\mathrm{A.I.}\left(\frac{1}{4}\right) = \frac{v_{\mathrm{R}}\left(\frac{1}{4}\right) + v_{\mathrm{B}}\left(\frac{1}{4}\right) - 2c(9/10)}{v_{\mathrm{R}}\left(\frac{1}{4}\right) - v_{\mathrm{B}}\left(\frac{1}{4}\right)}$$

where $v_{\mathrm{B}}\left(\frac{1}{4}\right)$ and $v_{\mathrm{R}}\left(\frac{1}{4}\right)$ are the radial velocities measured on the blue and red sides of Hβ_{BC} at 1/4 fractional intensity. The asymmetry index thus defined is independent of assumptions about the rest frame. In general, we define a centroid radial velocity as

$$c\left(\frac{i}{4}\right) = \frac{v_{\mathrm{R}}\left(\frac{i}{4}\right) + v_{\mathrm{B}}\left(\frac{i}{4}\right)}{2},$$

which we list in Table 3 for $i = 1$ and 3. In the definition of A.I., we use $c\left(\frac{9}{10}\right)$ as a proxy for the peak radial velocity $c\left(\frac{4}{4}\right)$.

The optical Eigenvector 1 parameters ($R_{\mathrm{FeII}} = W(\mathrm{Fe\,II}\lambda4570)/W(\mathrm{H}\beta_{\mathrm{BC}})$ and $FWHM(\mathrm{H}\beta_{\mathrm{BC}})$; S00b) can be computed from the data in Tables 2 and 3. Figure 4 shows the location of the low and intermediate-redshift quasars in the optical plane of E1. The VLT/ISAAC sources show no significant difference in E1 domain space occupation. In contrast Mc99 data suggests a rather different picture with most sources located in an "outlier" region that is scarcely populated by low-redshift AGN: $FWHM(\mathrm{H}\beta_{\mathrm{BC}}) \gtrsim 10\,000$ km s^{-1}. No low-redshift sources are observed with the additional condition $R_{\mathrm{FeII}} \gtrsim 0.5$, where ≈10 of the Mc99 sources are found.

Table 3. H$\beta_{\rm BC}$ line profile measurements.

Source (1)	*FWZI*[a] (2)	$\Delta^{a,b}$ (3)	*FWHM*[a] (4)	$\Delta^{a,b}$ (5)	*A.I.*[c] (6)	Δ^{b} (7)	Kurt.[d] (8)	Δ^{b} (9)	$c(1/4)$ (10)	$\Delta^{a,b}$ (11)	$c(1/2)^{a}$ (12)	$\Delta^{a,b}$ (13)	$c(3/4)^{a}$ (14)	$\Delta^{a,b}$ (15)	$c(0.9)^{a}$ (16)	$\Delta^{a,b}$ (17)
HE0003−5026	20 500	400	5400	400	−0.02	0.10	0.32	0.05	−1300	900	−250	410	−520	270	−520	180
HE0005−2355	20 100	3100	5900	600	0.27	0.06	0.28	0.03	3000	800	1180	620	410	320	20	190
HE0048−2804	19 700	3400	7500	400	0.04	0.10	0.44	0.06	300	1100	590	390	820	420	−90	360
HE0122−3759	12 100	2800	3400	300	−0.08	0.06	0.33	0.04	−500	300	−100	300	−30	170	−20	110
HE0205−3756	22 200	1800	5100	500	0.34	0.08	0.22	0.04	2600	1200	−310	480	−680	170	−510	130
HE0248−3628	21 200	1200	4200	300	−0.12	0.16	0.30	0.08	−800	1200	−330	340	−20	230	30	140
HE0331−4112	17 700	1300	5500	300	0.00	0.11	0.39	0.07	1600	1000	990	310	840	280	820	210
HE0349−5249	24 700	2300	5100	600	0.46	0.08	0.20	0.04	7800	1900	1110	610	670	260	520	170
HE0454−4620	7700	300	3400	200	−0.20	0.08	0.43	0.05	1500	300	1120	250	...	150	160	110
HE2202−2557	22 600	1700	7000	500	0.16	0.10	0.34	0.06	1800	1300	930	490	280	360	−80	270
HE2259−5524	9700	1000	2900	200	−0.17	0.10	0.31	0.06	−800	500	−90	180	70	130	20	80
HE2305−5315	15 000	4900	3300	500	−0.17	0.09	0.20	0.04	−1100	700	−390	510	−110	180	20	80
HE2340−4443	13 700	300	4200	300	0.05	0.09	0.35	0.06	600	700	220	290	180	220	110	150
HE2349−3800	20 600	800	5200	500	0.34	0.09	0.34	0.06	2300	1000	930	470	−200	180	−410	130
HE2352−4010	14 700	2400	3200	300	−0.07	0.08	0.29	0.05	−400	500	−310	280	−90	180	−10	100
HE2355−4621	22 000	2300	6900	500	0.26	0.08	0.35	0.05	2900	1000	1320	460	390	440	−20	230

[a] In units of km s^{-1}.
[b] 2σ confidence level uncertainty.
[c] Asymmetry index defined as in Marziani et al. (1996).
[d] Kurtosis parameter as in Marziani et al. (1996).

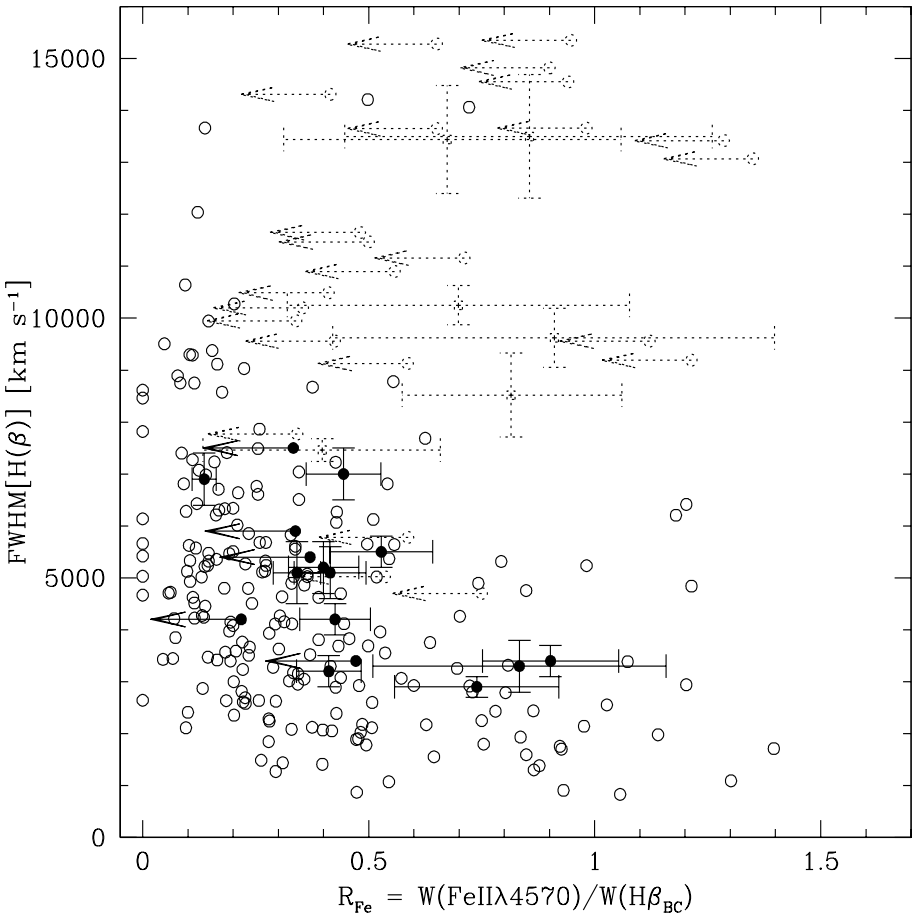

Fig. 4. Distribution of Seyfert 1 and quasars in the optical plane of E1, *FWHM*(H$\beta_{\rm BC}$) (in units of km s^{-1}) vs. $R_{\rm FeII}$. Open circles: M03, 215 AGN; filled circles: 17 VLT/ISAAC sources of the present study; open circles with dotted lines: 22 $z \approx 2.5$ sources studied by Mc99, with upper limits and uncertainties in $R_{\rm FeII}$ set according to M03.

Table 4. Results on C IVλ1549 and optical redshift comparison for sources with $z \geq 1.5$.

Source[a]	Pop.[b]	z^c(HE)	Shift[c] [km s^{-1}]	Notes
HE 0005−2355	B	1.405	−900	
HE 0122−3759	A	2.164	−3400	
HE 0205−3756	A	2.404	−3000	H$\beta_{\rm BC}$ profile of Pop. B; borderline
HE 0248−3628	A	1.516	−2400	
HE 2202−2557	B	1.5295	−600	
HE 2352−4010	A	1.540	−4600	very low W(C IVλ1549), extreme Pop. A
HE 2355−4621	B	2.380	−200	excellent spectrum; could be z(C IVλ1549$_{\rm BC}$) > z(C IVλ1549$_{\rm NC}$)

[a] Of the other sources with $z \gtrsim 1.5$, the spectrum of HE 0349−5249 is not available to us. The spectrum of HE 2349−3800 is too noisy even for rough shift measurements.
[b] Classification done according to the luminosity-dependent relationship $FWHM(M_B) \approx 500 \times 10^{(-0.08(M_{\rm B}+20.24))} + 3400$ km s^{-1}.
[c] Shift measured as $c[z(\text{C IV}\lambda1549) - z_{\rm opt}]/[1. + z_{\rm opt}]$, where $z_{\rm opt}$ is as reported in Table 1, and z(C IVλ1549) refers to a measurement of the upper half of the profile by Gaussian fitting. No attempt was made to deconvolve C IVλ1549$_{\rm BC}$ and C IVλ1549$_{\rm NC}$.

We suggest that the latter data sample is critically affected by poor *S/N* (Sect. 5.2).

Some general trends seen in the low-redshift data continue to be found: 1) RL sources favor Population B and show lower average $R_{\rm FeII}$ values; 2) *FWHM* H$\beta_{\rm BC}$ and $R_{\rm FeII}$ values do not differ significantly between Population B RL and RQ sources; 3) moving towards Population A we find the same systematic increase in average $R_{\rm FeII}$ (from 0.37 to 0.54); 4) Population A sources favor the upper envelope of the low redshift distribution which may be pointing to a correlation between $FWHM$(H$\beta_{\rm BC}$) and luminosity (see Sect. 5.2.1); and 5) C IVλ1549 measures show expected E1 trends as discussed in the next section.

4.1. CIVλ1549 trends for the VLT quasars

CIV profile shift was adopted as one of the E1 parameters rather than EW CIV because its interpretation is less ambiguous. Population A sources in the low-redshift sample show a systematic CIV blueshift while Population B sources do not. Population A sources also show a lower mean EW than Population B AGN (S00b). Optical ground-based C IVλ1549 spectra exist for three of the HE sources and they are discussed individually. In addition HE discovery spectra (courtesy of L. Wisotzki) for sources with $z \gtrsim 1.5$ include C IVλ1549. Table 4 summarizes the E1 CIV shift parameter for VLT sources with available data. Profile shift was measured relative to rest frame measures derived from [O III]$\lambda\lambda$4959,5007.

HE 0005−2355: We call this a Population B RL source. Espey et al. (1989) report $z \approx 1.411$ consistent with the general absence of large C IVλ1549 blueshifts in Population B sources (we obtain $z \approx 1.412$; Espey et al. 1989 report $z \approx 1.407$ for Hα with $FWHM$(H$\beta_{\rm BC}$) ≈ 5900 km s^{-1}). The more recent HE measure gives $z \approx 1.405$ but with CIV at the noisy blue edge of the spectrum.

HE 0122−3759: Population A RQ source. Comparison of C IVλ1549 redshifts (2.173: Carswell et al. 1982; 2.178: Espey et al. 1989) with our [O III]$\lambda\lambda$4959,5007 value (2.200) suggest a large blueshift. Espey et al. (1989) derive $z = 2.207$ from Hα and $z \approx 2.199$ from Mg IIλ2800. An HE spectrum (CIV $z \approx 2.164$) confirms the large blueshift $C \sim -3400$ km s^{-1} with an amplitude seen only in extreme Population A (i.e. NLSy1) sources. The highest amplitude blueshifts at high and low redshift fall in the range $C \approx -4000 \div -5000$ km s^{-1} (S00b; Richards et al. 2002).

HE 0205−3756: Population A RQ source. A published C IVλ1549 measure yields $z \approx 2.395$ (Ulrich 1989). This implies a large blueshift $C \sim 3000$ km s^{-1} relative to our rest frame measure $z = 2.437$ (2.412 in Wilkes 1986). The low measured W(C IVλ1549) (Ulrich 1989) is also consistent with a Population A source (S00b). Taken at face value, EW and profile shape for H$\beta_{\rm BC}$ appear characteristic of Population B. However the H$\beta_{\rm BC}$ red shelf may be a spurious feature caused by residuals from the very strong sky lines. Either this object is affected by bad data or it may herald a change towards more "population ambiguous" quasars at high redshift/luminosity that must be monitored as our sample increases.

In summary we confirm that C IVλ1549 blueshifts first observed by Gaskell (1982) may be increasingly common in intermediate redshift quasars. All certain blueshifts in the VLT HE sample are found in Population A sources as predicted from E1, while all Population B shifts are marginal (see Table 4).

4.2. Luminosity trends

Studies of the E1 parameter space have thus far been constrained to sources with $z < 1.0$ and mostly $M_B \gtrsim -25.0$. The redshift constraint reflects the loss of the Hβ spectral region to optical observation at $z \gtrsim 1.0$. The magnitude constraint reflects our *S/N* and resolution requirements convolved with telescopes readily available to us. Lower-quality data cannot provide accurate E1 parameter measures or reveal E1 domain occupation clearly. The analogy would be to try to define the H-R diagram for a star cluster using magnitudes and $B - V$

Table 5. Results of luminosity correlation analysis.

Parameters[a]	Sample[b]	Spearman's ρ[c]		
		All	RQ[d]	RL[d]
(1)	(2)	(3)	(4)	(5)
FWHM	M03	−0.159 (0.020)	−0.066 (0.418)	0.092 (0.463)
FWHM	M03+VLT/ISAAC	−0.165 (0.012)	−0.105 (0.183)	0.087 (0.475)
FWHM	PG+VLT/ISAAC	−0.330 (0.001)	−0.261 (0.016)	0.155 (0.561)
$R_{\rm FeII}$ UL	M03	0.222 (0.001)	0.087 (0.290)	0.159 (0.202)
$R_{\rm FeII}$ UL	M03+VLT/ISAAC	0.160 (0.015)	0.038 (0.623)	0.079 (0.515)
$R_{\rm FeII}$ UL	PG+VLT/ISAAC	0.069 (0.489)	−0.011 (0.922)	−0.017 (0.951)
$W(\rm H\beta_{BC})$	M03	−0.073 (0.288)	−0.136 (0.096)	0.088 (0.481)
$W(\rm H\beta_{BC})$	M03+VLT/ISAAC	−0.056 (0.734)	0.088 (0.2695)	0.029 (0.810)
$W(\rm H\beta_{BC})$	PG+VLT/ISAAC	0.169 (0.090)	0.090 (0.4015)	0.689 (0.010)
W(FeIIλ4570) UL	M03	0.199 (0.004)	−0.019 (0.8184)	0.156 (0.213)
W(FeIIλ4570) UL	M03+VLT/ISAAC	0.184 (0.005)	−0.001 (0.990)	0.174 (0.157)
W(FeIIλ4570)	PG+VLT/ISAAC	0.130 (0.191)	−0.021 (0.847)	0.439 (0.100)
W([OIII]λ5007)	M03	0.300 ($<10^{-4}$)	0.464 ($<10^{-4}$)	0.317 (0.012)
W([OIII]λ5007)	M03+VLT/ISAAC	0.375 ($<10^{-4}$)	0.541 ($<10^{-4}$)	0.319 (0.009)
W([OIII]λ5007)	PG+VLT/ISAAC	0.332 (0.001)	0.423 (0.0001)	0.300 (0.261)

[a] Correlated against M_B ($q_0 = 0$; $H_0 = 75$ km s^{-1} Mpc^{-1}).
[b] M03: 215 objects in Marziani et al. (2003a); VLT/ISAAC: 17 observations of this paper.
[c] Computed with the assumption that FeIIλ4570 upper limits (UL) are censored data. If no UL are present, ρ is equal to the Spearman's rank correlation coefficient r. In parenthesis, we report the probability that a correlation is not present.
[d] M03: 65 RL, 150 RQ; M03+VLT/ISAAC: 69 RL, 162 RQ; PG+VLT/ISAAC: 102 (85 PG) sources; 87 RQ and 15 RL.

colors with respective uncertainties of ±1.0 and ±0.4. This issue would be irrelevant if all quasars were alike but source occupation in the E1 domain (in analogy to stars in the H-R domain) is not random and the difference between so-called Population A and B quasars is found in virtually all AGN properties (see also Sulentic et al. 2002). Within our sample constraints, optical luminosity is uncorrelated with E1 properties at low redshift (S00b; M03b).

Beyond tests of the robustness of E1 space, extension of our sample to higher redshift/luminosity can address many questions. Do quasars maintain the same emission line properties over the full range of redshift/luminosity? Can we constrain any form of evolution?

In particular, can we identify any difference in optical FeII$_{\rm opt}$ emission? Is the evolution of quasar spectral parameters consistent with the expectations of broadening by virial motions? We will address these questions, as far as currently possible, one parameter at a time. Table 5 provides a synopsis of our luminosity correlation analysis. We report the generalized Spearman rank correlation coefficient computed for the general case of censored data (Isobe et al. 1986). M03b data yield only meaningful upper limits for FeIIλ4570 and $R_{\rm FeII}$ for several tens of sources. Of course, whenever upper limits are not considered the correlation coefficient reduces to the usual Spearman r. We also considered the PG quasar sample independently as well as the VLT/ISAAC data and, with a single exception (see Sect. 4.2.1), found behavior in agreement with those of the other samples (albeit the PG RL sub-sample ($n = 15$) is too small to give reliable correlation coefficients). No credible evidence for a luminosity correlation was found.

4.2.1. E1 broad line parameters

FWHM(H$\beta_{\rm BC}$): Fig. 5a shows the M03b+VLT source distributions in the *FWHM*(H$\beta_{\rm BC}$) vs. M_B plane. Early, as well as recent, works (e.g., Joly et al. 1985; Corbett et al. 2003) suggested at most a weak correlation between *FWHM*(Hβ) and source luminosity. A weak tendency for *FWHM*(H$\beta_{\rm BC}$) to increase with M_B was also suspected in the M03b data. The weakness of the "correlation" is quantified by the Spearman correlation coefficients (≈−0.15) for the M03b+VLT/ISAAC sample. Any weak trend in this plot disappears completely if we correct for a correlation induced because RL sources in our sample tend to have higher mean luminosity and *FWHM*(H$\beta_{\rm BC}$) than RQ sources. The most significant feature of the plot involves an apparent systematic increase in the smallest observed *FWHM* with increasing M_B. *FWHM*(H$\beta_{\rm BC}$) increases from 1000 to 3000 km $^{-1}$ between $M_B = -23$ and -28. Very broad Hβ profiles are observed at all luminosities although sources with *FWHM*(H$\beta_{\rm BC}$) > 10^4 km s^{-1} appear to be quite rare and possibly disjoint with respect to the bulk of the sample. This sparseness is likely physically motivated because sources with large *FWHM*(H$\beta_{\rm BC}$) and W(H$\beta_{\rm BC}$) really exist and are not the product of observational errors. Such sources are sometimes double-peaked (Eracleous & Halpern 2003, and references therein) and are also

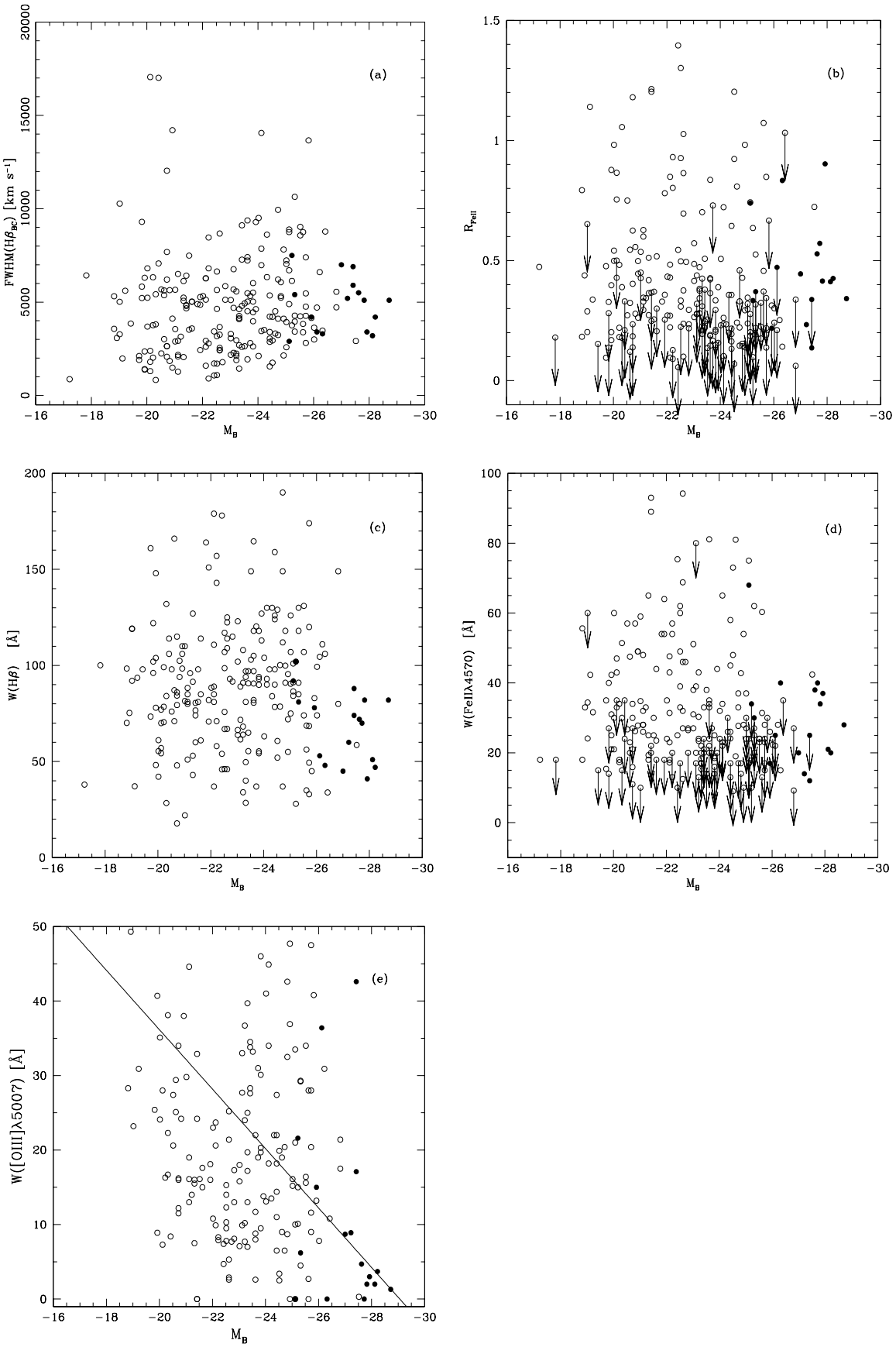

Fig. 5. *FWHM*(H$\beta_{\rm BC}$), $R_{\rm FeII}$, W(H$\beta_{\rm BC}$), W(Fe IIλ4570), and W([O III]λ5007) vs. absolute blue magnitude M_B. Equivalent widths are in the rest frame, in units of Å; *FWHM*(H$\beta_{\rm BC}$) is in km s^{-1}. Open circles: M03 data; filled circles: VLT/ISAAC sources. Best fit according to a robust method is provided in the only case of a significant correlation.

somewhat unstable systems that may be radiating at very low *L/M* in the E1 context and may therefore be intrinsically short-lived (Sulentic et al. 1995; Marziani et al. 2001).

$R_{\rm FeII}$: the second E1 optical parameter $R_{\rm FeII}$ shows no convincing evidence (Fig. 5b) for a correlation if RQ and RL sources are considered separately (RL are weaker Fe II$_{\rm opt}$ emitters than RQ sources, which accounts for the somewhat larger correlation coefficient when no RQ-RL distinction is made). The $R_{\rm FeII}$ situation is however more complicated because many W(Fe IIλ4570) measurements are actually upper limits. We therefore considered two cases: 1) we used the best fit Fe IIλ4570 estimates from M03b + Table 2; and 2) we used minimum values of Fe IIλ4570 detectability (which depend on *FWHM* and *S/N*) to derive Fe IIλ4570 upper limits. We then performed a censored data analysis computing Kendall's τ, in addition to Spearman r, as an estimator of the correlation. Similar results are found in the two cases (τ values are not reported).

4.2.2. W(H$\beta_{\rm BC}$) and the H$\beta_{\rm BC}$ profile

Claims that W(H$\beta_{\rm BC}$) decreases with luminosity have been rather unconvincing due to small sample sizes and large intrinsic scatter (Sulentic et al. 2000a, and references therein (no); Mc99 (no); Wilkes et al. 1999 (yes); Croom et al. 2002 (no)). In the M03b+VLT samples W(H$\beta_{\rm BC}$) shows no significant correlation with M_B even if RQ and RL subsamples are combined (in contrast to $R_{\rm FeII}$ and *FWHM*(H$\beta_{\rm BC}$)). It is however intriguing that W(H$\beta_{\rm BC}$) measured for VLT sources are all $\lesssim$100 Å (Fig. 5c).

Table 3 reports line profile measures for 16/17 VLT sources. HE 0353−3919 is excluded because H$\beta_{\rm BC}$ falls in the gap between the *sZ* and *Z* bands allowing only a rough estimate of *FWHM*(H$\beta_{\rm BC}$) $\sim$ 6000 km s^{-1}. We considered the luminosity dependence of AI, c(1/4), and c(3/4) which are the most robust parameters (least affected by errors; M96). No significant correlation was found.

4.2.3. Fe II$_{\rm opt}$ emission properties

Figure 5d shows no evidence for a correlation between M_B and W(Fe IIλ4570). The absence of a W(Fe IIλ4570) trend is less significant because of the larger uncertainty associated with these measures. In modeling and subtracting Fe II$_{\rm opt}$ emission we found no source that significantly deviated from the scaled and broadened I Zw 1 template. This template is remarkably successful for modeling even sources with strong and narrow Fe II$_{\rm opt}$ emission such as HE 2305−5315 and HE 0122−3759. It also works well for sources with obviously broader lines (e.g. HE 0248−3628). We found no convincing examples of unusual Fe II$_{\rm opt}$ emission (i.e. multiplet ratios different from I Zw 1).

FWHM(H$\beta_{\rm BC}$) and *FWHM*(Fe IIλ4570) are strongly correlated as shown in Fig. 7. This is consistent with the hypothesis that profiles of individual Fe IIλ4570 lines are very similar to H$\beta_{\rm BC}$. A weighted least-squares fit yields a slope of $\approx$1.31 ± 0.22 (1σ uncertainty). The large uncertainty reflects the relative insensitivity of the template fits to the adopted line width.

4.2.4. Narrow lines

The VLT sample shows a large number of sources with weak [O III]$\lambda\lambda$4959,5007 emission. Figure 5e shows the best fit for all sources (M03+VLT/ISAAC) using a robust fitting method. While this fit tells us little or nothing, we do see an interesting difference between the M03b and VLT samples. The M03b sample shows a large range in W([O III]$\lambda\lambda$4959,5007) at all luminosities. Most of the VLT measures cluster at very low values. The values are low even relative to the M03b sample that contains a significant number of NLSy1 sources. They are as low or lower than measured values for extreme Population A blue outlier sources (Marziani et al. 2003a). This may be the first hint of a real decrease in the strength of the narrow line region for higher luminosity quasars.

5. Discussion

5.1. The E1 parameter space

The so-called E1 parameter space is a reasonable approximation to a (4D) H-R Diagram for AGN (S00b). In this context we mean: 1) discrimination between and unification of the diverse classes of AGN and, possibly; 2) representation of various states of source spectral evolution. If an H-R analogy is in any way useful, it would not be surprising to find that more than two observational parameters are required to define it. We take it as a given that a quasar H-R Diagram is needed because of the striking diversity in the spectral signatures of the broad line regions for different AGN classes (S00b; Sulentic et al. 2002). It is hoped that the E1 parameter space will both clarify the phenomenology and better focus models for the central geometry and physics. One of the big challenges for E1 is to remove the degeneracy between physics and source orientation to our line of sight (Sulentic et al. 2003). Right now, in analogy to mass (M) as the physical driver of the stellar main sequence, evidence suggests that the Eddington ratio ($\propto \dot{M}$) is the principal physical driver in E1 (Marziani et al. 2001; M03b; Boroson 2002). As an equivalent to the stellar main sequence we find an "L-shaped" distribution of points in the optical parameter plane of E1 (*FWHM*(H$\beta_{\rm BC}$) vs. $R_{\rm FeII}$; Fig. 4). The present tentative results suggest that the L-shaped distribution is preserved up to $M_B \approx -30$. We have earlier suggested that the extreme Population A sources with the narrowest Balmer profiles, strongest FeII emission, CIV blueshift and soft X-ray excess are the high accretion end of the E1 sequence (S00b). We also suggested that these extreme objects may represent the quasar "seed" population (see also Mathur 2000). In this context we expect the fraction of such extreme sources to increase with redshift. Both the SDSS CIV (Richards et al. 2002) and initial VLT samples are consistent with this idea (i.e. high frequency of CIV blueshifts at high redshifts and weak narrow line regions at intermediate redshifts, respectively). Overall however the VLT sample follows closely the low-redshift E1 results.

5.2. The need for high S/N and resolution

The Mc99 data pose an apparent challenge to our claims about E1 robustness at higher redshifts. Unfortunately, the Mc99 data have very low *S/N*. Even if the spectral resolution (≈530 km s^{-1}) is modestly reasonable, the *S/N* is in general ≲10 (see their Sect. 2 and Table 1). It is very risky to measure Fe II$_{opt}$ emission in data with such low *S/N* and limited spectral coverage. M03b estimated the minimum detectable W(Fe IIλ4570) as a function of $FWHM$(Hβ_{BC}) for several *S/N* values. For *S/N* ≈ 10 we find the approximate relation: $W(\mathrm{Fe\,II}\lambda4570)_{min} \approx 25 + 0.017\,FWHM(\mathrm{H}\beta_{BC})$, where the rest frame W(Fe IIλ4570) is in Å, and $FWHM$(Hβ_{BC}) is expressed in km s^{-1}. $W(\mathrm{Fe\,II}\lambda4570)_{min} \approx 50$ Å for $FWHM(\mathrm{H}\beta_{BC}) \approx 13\,000$ km s^{-1}, which explains why we have so many upper limits among the Population B sources. Most R_{FeII} values reported by Mc99 should be changed to upper limits. We simulated Mc99 data with *S/N* ≈ 7 (sources Q0049+007, Q0153+257, Q1011+091, Q1309−056) with line widths and W(Fe IIλ4570) (always ≳60 Å) as given in that paper. We then set the R_{FeII} uncertainty to the upper limit $W(\mathrm{Fe\,II}\lambda4570)_{min}$ needed for a detection (i.e. upper limit is equal to the 3σ uncertainty) based on the errors in W(Hβ_{BC}) and $FWHM$(Hβ_{BC}) reported by Mc99. Even if Fe II$_{opt}$ is detected, the limited spectral coverage makes results very sensitive to the somewhat arbitrary continuum placement (e.g., Q1011+091). Some results are obviously arbitrary (e.g. Q0049+007 and Q0226−104) and there is no convincing evidence that lines are very broad or that Fe IIλ4570 should have W(Fe IIλ4570) ∼ 70 Å. Another doubtful case involves Q1209–056 although, again, the limited spectral coverage makes Fe II$_{opt}$ fitting an extrapolation for the blue and red blends. If upper limits and revised uncertainties are considered, the E1 quasar distribution in Fig. 4 can be significantly displaced toward $R_{FeII} \lesssim 0.5$. The same concerns apply to Yuan & Wills (2003) where both *FWHM* Hβ and R_{FeII} values are likely overestimated for many sources. Taken at face value the Mc99 quasars would imply very large black hole masses ($M_{BH} \sim 10^{11}\ M_\odot$) since they likely radiate at very low Eddington ratio (∼0.01–0.1) (Zamanov & Marziani 2002). Such large masses may not be frequent even among high-redshift quasars (McLure & Dunlop 2004).

5.3. A luminosity/mass dependent minimum $FWHM(H\beta_{BC})$?

Two of our VLT Population A sources (HE 0122−3759 and HE 2305−5315) show R_{FeII} (0.9 and 0.8) and no W([O III]$\lambda\lambda$4959,5007) detections. CIV data exists only for the former where an extreme CIV blueshift is measured. We call such sources extreme Population A or NLSy1 sources based on these criteria. The sources show $FWHM$(Hβ_{BC}) (3600 and 3200 km s^{-1} respectively) which significantly exceeds the nominal $FWHM(\mathrm{H}\beta_{BC}) \lesssim 2000$ km s^{-1} limit for NLSy1 sources. Such broader-lined and strong R_{FeII} Population A sources are also found in our low-redshift sample. The smallest c(Hβ_{BC}) ≈ 2600 km s^{-1} found among our 6 VLT Population A sources is larger than the *FWHM* of more than half of the Population A sources in our low-redshift sample. This suggests a possible lower limit to this parameter that is rising with source luminosity. HE 0122−3759 at $z \approx 2.4$, interpreted as an NLSy1, would be the most luminous yet observed. No X-ray detections are reported for these two sources.

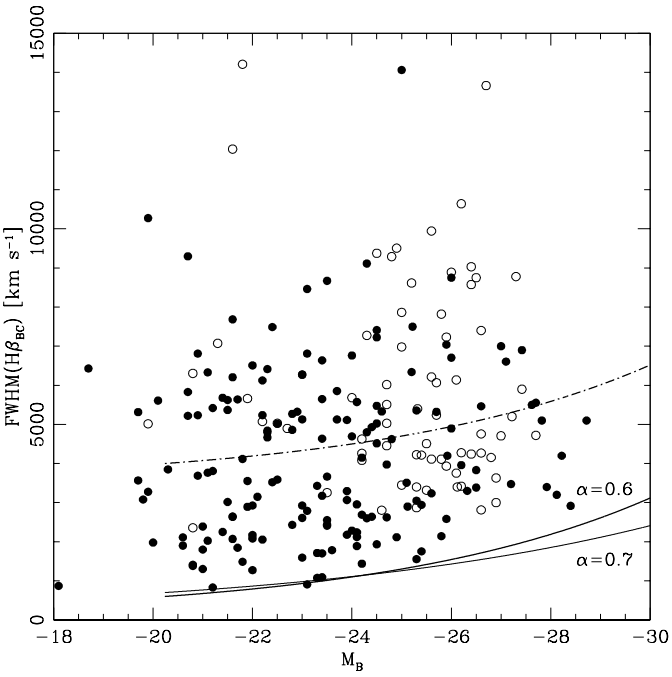

Fig. 6. $FWHM$(Hβ_{BC}) vs. M_B for the M03+VLT/ISAAC 232 sources, with RQ (filled circles) and RL (open circles) identified. The thick lines are the predicted minimum $FWHM$(Hβ_{BC}), as described in Sect. 5.3 (solid line), and the boundary between Populations A and B (dot-dashed line). The thin line refers to a slightly different fit to the $R_{BLR} - L$ relationship, with $\alpha = 0.7$.

In order to ascertain whether there is a luminosity effect, one can consider the well-defined lower boundary in the $FWHM$(Hβ_{BC}) vs. M_B diagram (Figs. 5a and 6). This boundary can be interpreted as a luminosity effect. Such a trend is indeed expected if: 1) Hβ_{BC} broadening is dominated by virial motions and 2) the emissivity-weighted distance of the BLR from the central BH depends on luminosity $R_{BLR} \propto L^{-\alpha}$ (Kaspi et al. 2000). The exact value of α is very sensitive to: a) the poor sampling in some luminosity ranges; b) the presence of several outliers; and c) the cosmology (Marziani et al. 2003a). Refitting Kaspi's data for $H_0 = 75$ km s^{-1} Mpc^{-1} and $q_0 = 0$, we obtain:

$$R_{BLR} \approx 1.19 \times 10^{17} \left(\frac{L}{10^{45}}\right)^{0.60} \text{ cm}$$

where we have assumed that the bolometric luminosity $L \approx 10\lambda L_\lambda$ at 5100 Å. The value of $\alpha = 0.7$ is slightly different from the value given by Kaspi et al. (2000).

The virial relationship implies:

$$\frac{\sqrt{3}}{2} FWHM = G^{\frac{1}{2}} M^{\frac{1}{2}} R_{BLR}^{-\frac{1}{2}}$$

where the factor 1/2 comes from the use of $FWHM$(Hβ_{BC}) ($\Delta v = \frac{1}{2} FWHM$) and the factor $\sqrt{3}$ takes into account that we measure a radially projected velocity. Substituting R_{BLR} with L and transforming into convenient units, we obtain:

$$FWHM(\mathrm{H}\beta_{BC}) \approx 2880\, L_{\odot,11}^{0.20} \left(\frac{L}{M}\right)_{\odot,3}^{-\frac{1}{2}} \text{ km s}^{-1}$$

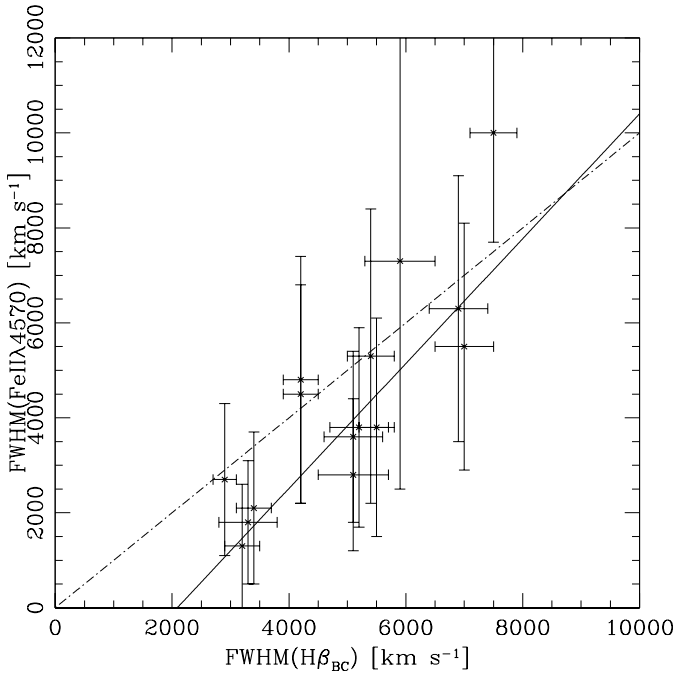

Fig. 7. *FWHM*(Fe IIλ4570) vs. *FWHM*(Fe IIλ4570) for the 17 VLT/ISAAC sources. The dot-dashed line traces the locus of *FWHM*(H$\beta_{\rm BC}$) = *FWHM*(Fe IIλ4570), while the continuous line is a least-squares best fit.

where luminosity is in 10^{11} $L_\odot$ and the L/M ratio is in units of 10^3 times the solar value ($L/L_{\rm Edd}$ = 1 corresponds to $\log\left(\frac{L}{M}\right)_\odot \approx 4.53$).

We add here the assumption that low-redshift NLSy1 with the narrowest lines radiate very close to the Eddington ratio. If we assume $\log\frac{L}{M} \approx 4.5$ we obtain $FWHM(\mathrm{H}\beta_{\rm BC})_{\rm min} \approx 600$ km s^{-1} for $\log L = 11$. The same relationship written for $\log L = 11$ as a function of M_B becomes:

$$FWHM_{\rm min}(\mathrm{H}\beta_{\rm BC}) \approx 500 \times 10^{[-0.08(M_{\rm B}+20.24)]} + 100 \text{ km s}^{-1} \propto 10^{(-0.08 M_{\rm B})}.$$

Considering the typical instrumental width of our data the actual $FWHM(\mathrm{H}\beta_{\rm BC})_{\rm min}$ would be ~1000 km s^{-1}. $FWHM(\mathrm{H}\beta_{\rm BC})_{\rm min}$ is similar to the lowest $FWHM(\mathrm{H}\beta_{\rm BC})$ found in the M03b sample. It is even closer to the lowest known $FWHM(\mathrm{H}\beta_{\rm BC})$ for NLSy1s (PHL 1092 and IRAS 13224−3809; Marziani et al. 2001). If we consider the luminosity dependence of $FWHM(\mathrm{H}\beta_{\rm BC})_{\rm min}$, we see that the expected trend for $\alpha = 0.6$ reproduces fairly well the $FWHM(\mathrm{H}\beta_{\rm BC})$ lower boundary as a function of M_B, especially if we consider only RQ sources (see Fig. 6). A less pronounced trend is expected for $\alpha = 0.7$, especially at high luminosity. This result is helpful for interpreting the following three issues:

Correlation of $FWHM(\mathrm{H}\beta_{\rm BC})$ with luminosity: A significant correlation between *FWHM* and luminosity may depend on: 1) sample selection; and 2) intrinsic dispersion of *FWHM* values in a narrow M_B range. It will also be affected by the fact that the profile of Hβ is now known to be composed of at least three independent components; narrow, broad and very broad (Sulentic et al. 2002). Population A sources appear to be dominated by the "classical" broad component. Population B can be significantly affected by the unshifted narrow and redshifted very broad components. In many sources these two components can cancel any bias on the measured *FWHM* H$\beta_{\rm BC}$. In others they do not and resultant *FWHM* measures cannot be safely compared with the above or Population A sources. Given the low *S/N* of most quasar spectra, the very broad component will often be modelled with the continuum. *FWHM* measures for such sources will often be serious underestimates unless the narrow component is explicitly subtracted. This leads to a prediction that RL sources (mostly Population B) will be systematically measured with *FWHM* (and consequently, $M_{\rm BH}$) too low in low *S/N* spectra.

One must consider that any expected *FWHM*-luminosity dependence will be very weak. This means that it is reasonable to expect an increase $\Delta FWHM(\mathrm{H}\beta_{\rm BC}) \approx 1000$ km s^{-1} over an increase of $\Delta M_B \approx 10$, with $FWHM(\mathrm{H}\beta_{\rm BC})_{\rm min}$ changing from 1000 km s^{-1} to 2000 km s^{-1}. In a narrow M_B range, the intrinsic spread of $FWHM(\mathrm{H}\beta_{\rm BC})$ measures ranges from 1000–10 000 km s^{-1}. This will tend to make any intrinsic correlation very weak. Larger samples at higher luminosity are needed to test these predictions. Corbett et al. (2003), analyzing a very large sample from the 2dF and 6dF redshift surveys, find a weak increase of Hβ line width with luminosity, with a slope ≈1.5–0.2 (Δv vs. $\log L$), very close to the one expected from our calculation. However the average resolution, *S/N* and lack of FeII subtraction in this analysis warrant caution in accepting this result as support for our prediction. Higher luminosity/redshift spectra in this sample will show systematically lower *S/N*. If FeII-strong Population A sources really dominate at high redshift then most sources will have *FWHM* overestimated due in part to FeII blending with Hβ. Comparable (and reasonably high) *S/N* data are needed for sources at all redshifts and luminosities in order to make a proper luminosity correlation test.

RQ and RL differences: The $FWHM(\mathrm{H}\beta_{\rm BC})$ difference between RQ and RL sources is not simply a luminosity effect: if redshift and magnitude distributions are matched, RQ and RL still show systematic differences (M03b; Sulentic et al. 2003). This can also be seen restricting attention to higher luminosities ($M_B \lesssim -24$) where most RL are located: in this range $FWHM(\mathrm{H}\beta_{\rm BC})_{\rm RL} \gtrsim FWHM(\mathrm{H}\beta_{\rm BC})_{\rm RQ}$ (a Kolmogorov-Smirnov test indicates probability $P \sim 0.01$ that the *FWHM* values are drawn from the same distribution).

Boundaries: Populations A-B and NLSy1s: If we accept a low-redshift boundary between Population A and B sources at $FWHM(\mathrm{H}\beta_{\rm BC}) \approx 4000$ km s^{-1}, then it may increase as a function of luminosity following a curve parallel to that for $FWHM(\mathrm{H}\beta_{\rm BC})_{\rm min}$. If this correction is applied, the frequency of Population A (10) and Population B (7) sources among the 17 VLT/ISAAC sources is consistent with the low-redshift sample (Population A should be ~60–65% of all sources; Marziani et al. 2003a).

6. Summary and conclusion

We present 17 VLT/ISAAC spectra of intermediate redshift quasars with resolution and *S/N* comparable to our M03b sample of ground-based spectra for low-redshift AGN. Quasar spectra in the $1 \lesssim z \lesssim 2.5$ range do not yet show appreciable E1 parameter differences from quasars with $z < 1.0$. No significant luminosity correlations with line parameters are found again in agreement with previous E1 inferences. The two most interesting effects found in this preliminary comparison involve: 1) a tendency for the minimum *FWHM* Hβ to increase from ~1000 km s^{-1} at $M_B = -20$ to ~3000 km s^{-1} at $M_B = -28$; and 2) most of our VLT sources show W([OIII]$\lambda\lambda$4959,5007) values equal to or less than those found for the low-redshift sample. The former effect can be accounted for by accretion theory while the latter may indicate a weakening of the narrow line region in higher redshift quasars. A comparison with the largest sample of previously published IR data (Mc99) indicates that high *S/N* and spectral resolution are required to obtain meaningful results. Further VLT/ISAAC observations will provide a unique window on the E1 parameter space at high luminosity and redshift.

Acknowledgements. We thank Lutz Wisotzki for providing us with the HE optical spectra.

References

Barth, A. J., Martini, P., Nelson, C. H., & Ho, L. C. 2003, ApJ, 594, L95
Boroson, T. A. 2002, ApJ, 565, 78
Boroson, T. A., & Green, R. F. 1992, ApJS, 80, 109
Carswell, R. F., Whelan, J. A. J., Smith, M. G., Boksenberg, A., & Tytler, D. 1982, MNRAS, 198, 91
Corbett, E. A., Croom, S. M., Boyle, B. J., et al. 2003, MNRAS, 343, 705
Croom, S. M., Rhook, K., Corbett, E. A., et al. 2002, MNRAS, 337, 275
Dietrich, M., Appenzeller, I., Vestergaard, M., & Wagner, S. J. 2002, ApJ, 564, 581
Eracleous, M., & Halpern, J. P. 2003 ApJ, 599, 886
Espey, B. R., Carswell, R. F., Bailey, J. A., Smith, M. G., & Ward, M. J. 1989, ApJ, 342, 666
Freudling, W., Corbin, M. R., & Korista, K. T. 2003, ApJ, 587, L67
Gaskell, C. M. 1982, ApJ, 263, 79
Grupe, D., Beuermann, K., Mannheim, K., & Thomas, H.-C. 1999, A&A, 350, 805
Hamann, F., & Ferland, G. 1999, ARA&A, 37, 487
Isobe, T., Feigelson, E. D., & Nelson, P. I. 1986, ApJ, 306, 490
Joly, M., Collin-Souffrin, S., Masnou, J. L., & Nottale, L. 1985, A&A, 152, 282
Kaspi, S., Smith, P. S., Netzer, H., et al. 2000, ApJ, 533, 631
Marziani, P., Sulentic, J. W., Dultzin-Hacyan, D., Calvani, M., & Moles, M. 1996, ApJS, 104, 37 (M96)
Marziani, P., Sulentic, J. W., Zwitter, T., Dultzin-Hacyan, D., & Calvani, M. 2001, ApJ, 558, 553
Marziani, P., Zamanov, R. K., Sulentic, J. W., & Calvani, M. 2003a, MNRAS, 345, 1133
Marziani, P., Sulentic, J. W., Zamanov, R., et al. 2003b, ApJS, 145, 199 (M03b)
Mathur, S. 2000, MNRAS, 314, L17
Matteucci, F., & Recchi, S. 2001, ApJ, 558, 351
McIntosh, D. H., Rix, H.-W., Rieke, M. J., & Foltz, C. B. 1999, ApJ, 517, L73 (Mc99)
McLure, R. J., & Dunlop, J. S. 2004, MNRAS, in press [arXiv:astro-ph/0310267]
Murayama, T., Taniguchi, Y., Evans, A. S., et al. 1998, AJ, 115, 2237
Oya, S., Iwamuro, F., Tsukamoto, H., & Maihara, T. 1998, PASJ, 50, 163
Richards, G. T., Vanden Berk, D. E., Reichard, T. A., et al. 2002, AJ, 124, 1
Sulentic, J. W., Marziani, P., Zwitter, T., & Calvani, M. 1995, ApJ, 438, L1
Sulentic, J. W., Marziani, P., & Dultzin-Hacyan, D. 2000a, ARA&A, 38, 521
Sulentic, J. W., Zwitter, T., Marziani, P., & Dultzin-Hacyan, D. 2000b, ApJ, 536, L5 (S00b)
Sulentic, J. W., Marziani, P., Zamanov, R., et al. 2002, ApJ, 566, L71
Sulentic, J. W., Zamfir, S., Marziani, P., et al. 2003, ApJ, 597, L17
Véron-Cetty, M.-P., & Véron, P. 2000, A catalogue of quasars and active nuclei (Garching: ESO)
Ulrich, M.-H. 1989, A&A, 220, 71
Wilkes, B. J. 1986, MNRAS, 218, 331
Wilkes, B. J., Kuraszkiewicz, J., Green, P. J., Mathur, S., & McDowell, J. C. 1999, ApJ, 513, 76
Williams, R. J., Pogge, R. W., & Mathur, S. 2002, AJ, 124, 3042
Wisotzki, L., Christlieb, N., Bade, N., et al. 2000, A&A, 358, 77
Yuan, M., & Wills, B. 2003, ApJ, 593, 11
Zamanov, R., & Marziani, P. 2002, ApJ, 571, L77
Zamanov, R., Marziani, P., Sulentic, J. W., et al. 2002, ApJ, 576, 9

Online Material

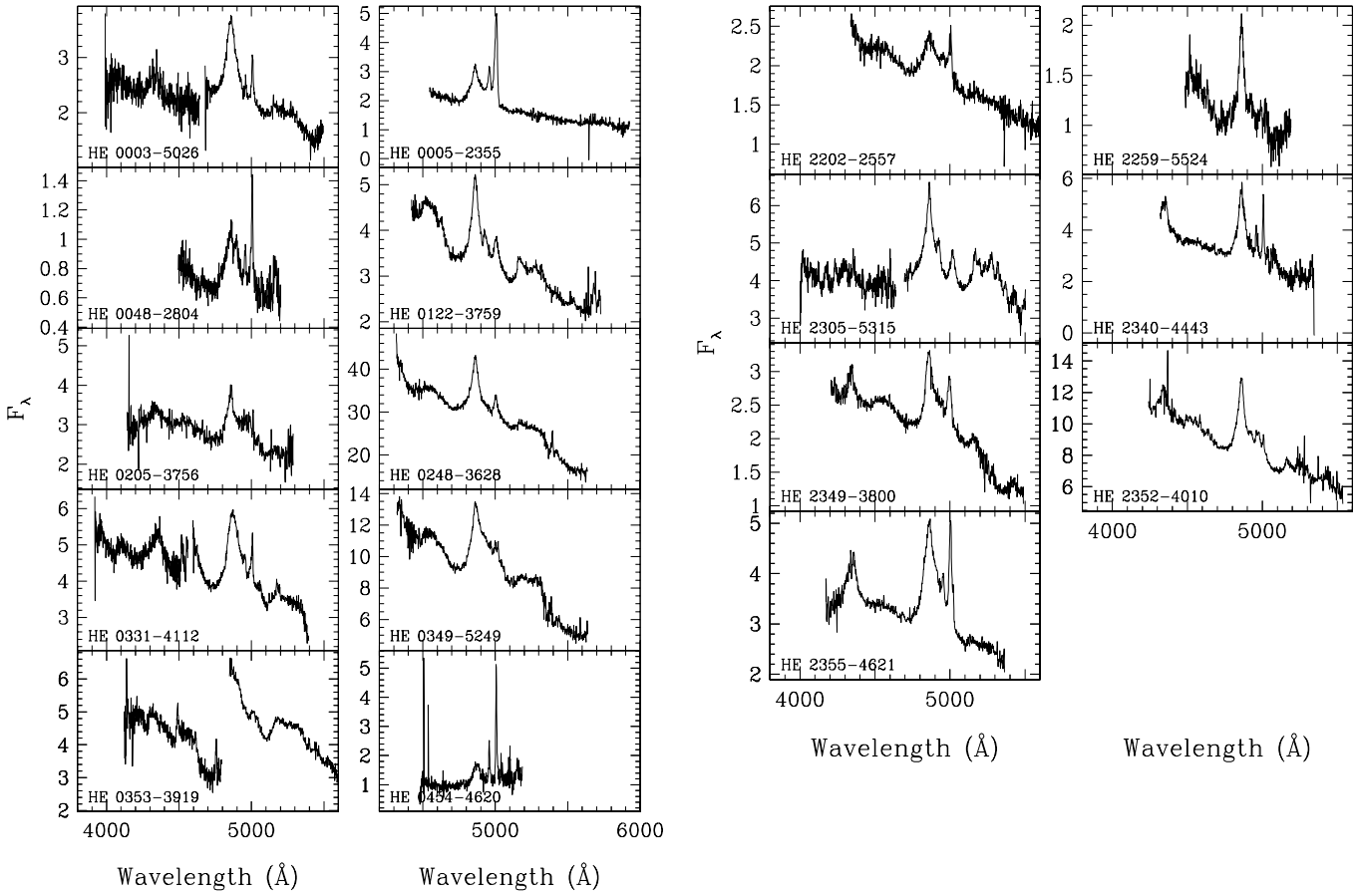

Fig. 1. Calibrated spectra of the 17 intermediate-redshift quasars. Abscissae are rest-frame wavelength in Å, ordinates are specific flux in units of 10^{-15} erg s^{-1} cm^{-1} Å^{-1}. Note that, for HE 0353−3919, ∼100 Å are missing in the blue side of the H$\beta_{\rm BC}$ profile, due to a gap between the *sZ* and *Z* bands.

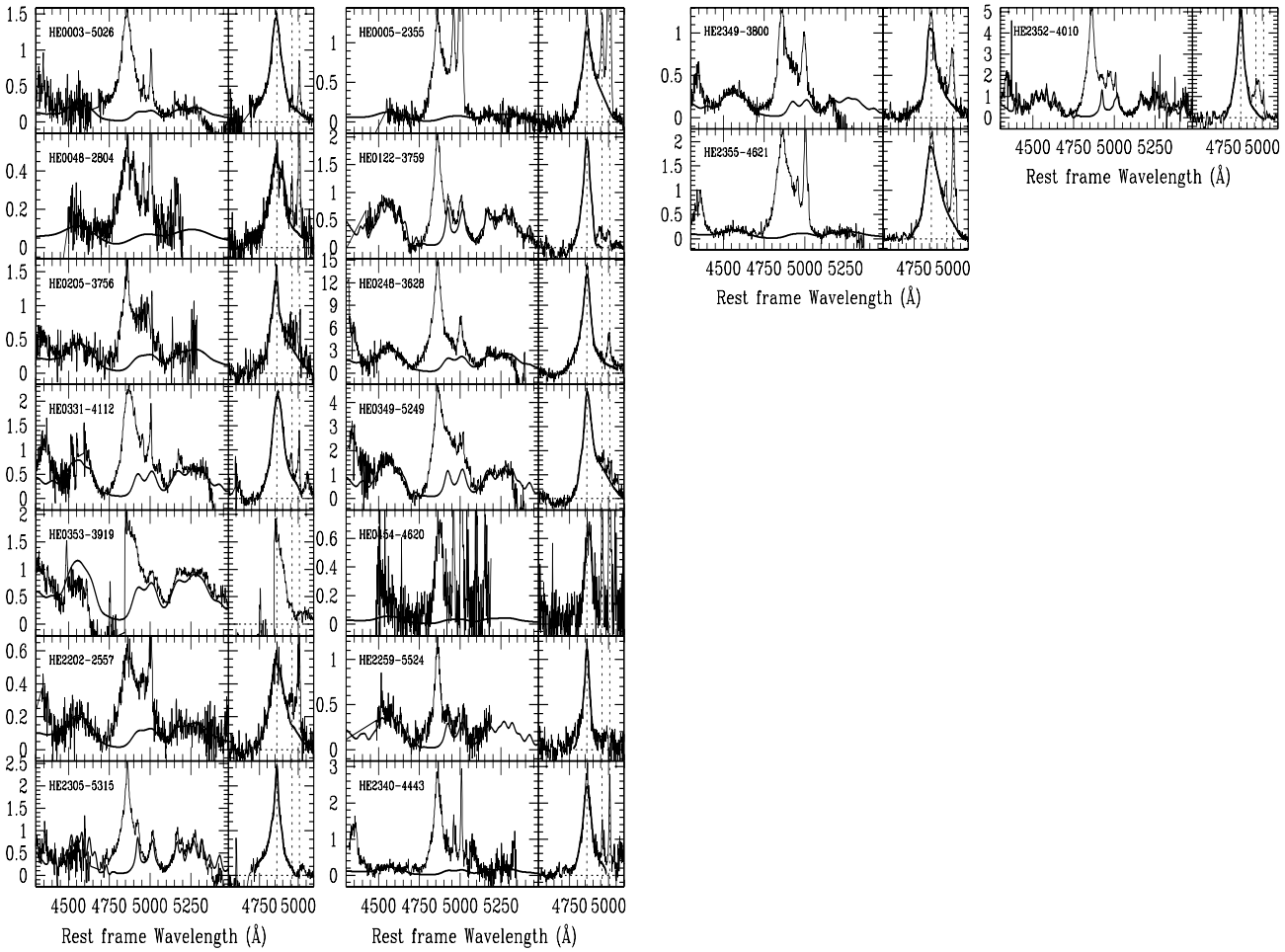

Fig. 2. Spectral atlas of the 17 intermediate-redshift quasars. The left panels show the continuum-subtracted Hβ spectral region. Abscissae are rest frame wavelength in Å, ordinates are specific flux in units 10^{-15} erg s^{-1} cm^{-1} Å^{-1}. The best-fit Fe II$_{opt}$ emission (see text) is traced as a thin (green) line. The right panels show an expansion around Hβ of the same spectrum after continuum and Fe II$_{opt}$ subtraction. Abscissae and ordinates are as above. The (blue and red) thick line shows a spline fitting of the pure Hβ_{BC} on the short and long wavelength side of the line respectively.

Table 1. Basic properties of sources and Log of observations.

Object name (1)	m_B^a (2)	z^b (3)	Line^c (4)	M_B^d (5)	log R_K^e (6)	Date^f (7)	Band^g (8)	DIT^h (9)	N_{exp}^i (10)	Airmass^j (11)	*S/N*^{k} (12)
HE0003−5026	17.07	1.0772(4)	1	−26.7	2.19	2001-12-23	*Z*	180	12	1.42-1.59	20
							sZ	180	12	1.27-1.38	∼5
HE0005−2355	16.94	1.4120(3)	2	−27.6	2.56	2001-11-22	*J*	120	24	1.01-1.07	15
HE0048−2804	17.25	0.8467(3)	1	−26.0	...	2001-12-17	*Z*	150	16	1.04-1.11	7
HE0122−3759	16.94	2.2004(4)	2	−28.9	...	2001-12-28	*SH*	180	12	1.05-1.09	15
HE0205−3756	17.17	2.4367(5)	2	−29.0	...	2002-12-16	*SH*	180	12	1.05-1.09	35
HE0248−3628	16.58	1.5362(4)	2	−28.2	0.84	2001-12-28	*J*	180	12	1.03-1.05	30
HE0331−4112	16.24	1.1153(4)	1,2	−27.6	...	2001-12-23	*Z*	180	12	1.25-1.39	30
							sZ	180	8	1.41-1.54	15
HE0349−5249	16.13	1.5384(4)	2	−28.7	...	2002-02-26	*J*	120	20	1.26-1.38	30
HE0353−3919	16.14	1.0065(35)	3	−27.5	1.49	2002-02-26	*Z*	180	12	1.41-1.62	30
							sZ	180	12	1.70-2.05	15
HE0454−4620	17.23	0.8528(3)	1	−25.9	3.37	2002-12-16	*Z*	150	18	1.25-1.40	5
HE2202−2557	16.71	1.5347(3)	2	−28.1	1.80	2001-10-05	*J*	120	12	1.06-1.03	20
HE2259−5524	17.09	0.8549(4)	2	−26.1	...	2001-10-05	*Z*	180	18	1.20-1.16	10
HE2305−5315	16.33	1.0733(4)	2	−27.5	...	2001-11-24	*Z*	120	12	1.21-1.25	35
							sZ	180	8	1.17-1.20	10
HE2340−4443	17.07	0.9216(3)	1,2	−26.3	...	2001-11-25	*Z*	180	20	1.07-1.13	20–5
HE2349−3800	17.46	1.6040(4)	2,4	−27.4	1.93	2001-11-25	*J*	180	12	1.10-1.17	35–15
HE2352−4010	16.05	1.5799(4)	2	−28.8	...	2001-10-05	*J*	180	12	1.04-1.03	60–35
HE2355−4621	17.13	2.3825(3)	1,2	−28.9	...	2001-11-24	*SH*	180	24	1.13-1.29	20

[a] Apparent *B* magnitude.
[b] Redshift, with uncertainty in parenthesis.
[c] Lines used for redshift calculations: 1: [O III]λ5007, 2: Hβ, 3: Fe IIλ4570, 4: Hγ.
[d] Absolute *B* magnitude, computed for $H_0 = 75$ km s^{-1} Mpc^{-1}, $q_0 = 0$, and *k*-correction spectral index $\alpha = 0.6$. Note that M_B values are not those reported in the Verón-Cetty & Véron (2000) catalogue, but have been computed from the apparent *B* magnitude provided in the HE survey tables.
[e] Decimal logarithm of the specific flux ratio at 6 cm and 4400 Å (effective wavelength of the *B* band).
[f] Date refers to time at start of exposure.
[g] Photometric band.
[h] Detector Integration Time (DIT) of ISAAC, in seconds.
[i] Number of exposures with single exposure time equal to DIT.
[j] Airmass at start and end of exposure.
[k] *S/N* at continuum level. Where two values are reported they are for the blue and red side of Hβ_{BC} respectively. The *S/N* value is with *N* estimated at a 2σ confidence level i.e., 2 rms.